In Crystallo Reactions with an Engineered Cytochrome P450 Peroxygenase

Joel H.Z. Lee[a], John B. Bruning[b] and Stephen G. Bell[a]*.

[a]Department of Chemistry, University of Adelaide, Adelaide, SA, 5005, Australia

[b]School of Biological Sciences, University of Adelaide, SA 5005, Australia

KEYWORDS Metalloenzymes; Cytochrome P450 enzymes; Peroxyenase activity; Protein engineering'; X-ray crystallography

ABSTRACT: The cytochrome P450 monooxygenases are a class of heme-thiolate enzymes that are able to insert oxygen into unactivated C-H bonds. These enzymes can be converted into peroxygenases via protein engineering which enables this activity to occur using hydrogen peroxide (H_2O_2) without the requirement for additional nicotinamide co-factors or partner proteins. This offers significant advantages in terms of applications and mechanistic studies. Here, we investigate whether soaking crystals of an engineered P450 peroxygenase with H_2O_2 enables the enzymatic reactions to occur within the crystal. A designed bacterial P450 peroxygenase, CYP199A4 (T252E variant), which has enhanced activity for the *O*-demethylation of 4-methoxybenzoic acid using H_2O_2 was used. Crystals of T252E-CYP199A4 in complex with 4-methoxybenzoic acid were soaked with different concentrations of H_2O_2 for varying times to initiate an *in crystallo O*-demethylation reaction. Crystal structures of T252E-CYP199A4 showed a distinct loss of electron density that was consistent with the O-demethylated metabolite, 4-hydroxybenzoic acid when compared to the crystal structures of the same enzyme with the 4-hydroxybenzoic acid product and the 4-methoxybenzoic acid substrate bound. The visualisation of enzymatic catalysis in action is challenging in structural biology and the ability to start and monitor the reactions of P450 enzymes, or their progress, *in crystallo* by simply soaking crystals with H_2O_2 will enable new information on intermediates, such as product bound structures, and the mechanisms of these oxygenase reactions to be obtained.

Introduction

Cytochrome P450 enzymes (P450s) are heme-thiolate monooxygenases that catalyse the selective insertion of one atom of dioxygen (O_2) into C-H bonds. This enables them to catalyse a wide variety of complex transformations including epoxidation, heteroatom oxidation, desaturation, dealkylations, and C-C bond cleavage and formation.[1] The sequence identity between and substrates of P450s from different families and species can vary widely but their overall structures are broadly conserved. Their spectroscopic properties are similar due to the heme catalytic centre.[2, 3] Much of our knowledge of these enzymes is derived from the first structurally characterised cytochrome P450, $P450_{cam}$, a stereoselective camphor hydroxylating enzyme from a *Pseudomonas* bacterium. [4-7] The X-ray crystal structures of many P450s from across a variety of different species have now been determined.[8-11]

The structures of the ligand-bound (substrate and inhibitors) and substrate-free P450 enzymes are accessible through X-ray crystallography. The other intermediates of the P450 catalytic cycle can be explored using other techniques. X-ray crystallographic structures of certain intermediates of P450 enzymes have been proposed but this these species are challenging to isolate in the multi-step catalytic cycle of these enzymes. For other enzymes the use of cryogenic temperatures and rapid-data collection techniques have enabled the trapping and characterisation of intermediates in enzyme-catalysed reactions *in crystallo*.[12] One major challenge in trapping such reaction intermediate in P450 enzymes is initiating the reaction in protein crystals. This is hampered by the need for external electron transfer partners and nicotinamide cofactors (NAD(P)H) to initiate reactions.[13] Others have attempted to overcome this by reducing a crystal of substrate-bound P450s with electrons from the X-ray beam and in certain instances this can result in oxidation.[14-16] This approach has also led to the proposed formation of electron density consistent with an oxyferryl (Cpd I), the main oxidant of the P450 catalytic cycle.[17 18]

An alternate strategy to initiating enzymatic reactions in protein crystals of P450 enzymes is the use of the peroxide shunt pathway.[19] The peroxide shunt pathway is able to generate Cpd I (Scheme 1) directly using hydrogen peroxide. A small number of P450s are able to use this pathway for catalysis to act as peroxygenases.[20-26] As this shunt pathways and these P450 peroxygenases only requires hydrogen peroxide (H_2O_2) to initiate reactions, it may be possible to trigger *in crystallo* P450 reactions by simply soaking the crystal with peroxide. This could then potentially be used to trap and study the reactive intermediates involved in these enzyme reactions.

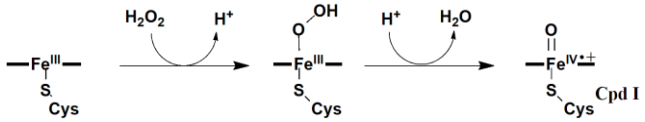

Scheme 1. The peroxide shunt pathway of P450 enzymes.

An attempt at capturing an *in crystallo* P450 enzyme reaction using hydrogen peroxide has been described previously.[27] A weak electron density corresponding to a hydroxylated hemiacetal intermediate was reported in the X-ray crystal structure of substrate-bound crystals of the P450 enzyme CYP121 after soaking with H_2O_2. A study with a peroxiredoxin enzyme also exploited a similar method to initiate *in crystallo* enzymatic reactions. Crystals of peroxiredoxin were soaked with H_2O_2 and structures were solved. Atomic resolution snapshots of the peroxiredoxin proceeding through thiolate, sulfenate, and sulfinate species were obtained.[28] Despite these studies efficient activation of heme oxygenases within crystals remains challenging.

CYP199A4 is a bacterial P450 enzyme from the bacterium *Rhodospeudomonas palustris* HaA2 that has high catalytic activity towards the oxidation of *para*-substituted benzoic acids.[29-32] The structure of CYP199A4 has been studied extensively by X-ray crystallography to elucidate the binding modes of various ligands and rationalise the activity this P450 enzyme.[33-36] CYP199A4 and its mutants have also been used as a model system to investigate mechanistic details of P450 reactions.[36-39] A rationally engineered variant of CYP199A4, the T252E mutant (T252E-CYP199A4), was found to have enhanced peroxygenase activity and is able use H_2O_2 for catalytic activity.[38, 40] A crystal structure of T252E-CYP199A4 complexed with 4-methoxybenzoic acid has been solved.[40] Given the enhanced peroxygenase activity of this P450 variant we hypothesise it should be able capable of *in crystallo* enzymatic reactions using hydrogen peroxide. By soaking crystals of T252E-CYP199A4 bound to its 4-methoxybenzoic acid with H_2O_2, we aim to assess if peroxygenase activity to oxidatively *O*-demethylate this substrate could occur within these crystals (Scheme 2).[40]

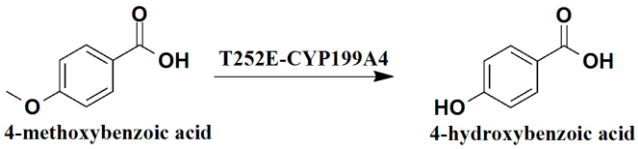

Scheme 2. The *O*-demethylation of 4-methoxybenzoic acid by CYP199A4.

Results

For *in crystallo* enzymatic reactions with T252E-CYP199A4, 4-methoxybenzoic acid was chosen as the substrate as it binds tightly to both the WT and T252E-CYP199A4 (K_d = 0.3 μM and 1.1 μM, respectively).[30 40] Protein crystals of T252E-CYP199A4 complexed with 4-methoxybenzoic acid were soaked with different concentrations of H_2O_2 to trigger the *in crystallo* reaction (0.5 - 10 mM H2O2 for 0 – 10 minutes). A total of 24 crystals of the T252E mutant were soaked in varying concentrations of H_2O_2 for different lengths of time and then flash-frozen in liquid N_2. X-ray diffraction data were collected. Three of these crystals showed high quality diffraction patterns.

Diffraction data of T252E-CYP199A4 co-crystallised with 4-hydroxybenzoic acid was also collected as a control to enable comparison to the H_2O_2-soaked crystals to both the substrate-bound (PDB 7REH) and product-bound structures. The structures of these crystals were determined and refined. The F_o-F_c difference maps were generated to assess negative and positive electron density around the bound molecule and confirm if *in crystallo* demethylation to generate 4-hydroxybenzoic acid occurred.

The structure of T252E-CYP199A4 co-crystallised with 4-hydroxybenzoic acid was solved and refined to a resolution of 2.03 Å (PDB: 8GLY). Structural refinement and data collection statistics were shown in Table S1. The overall protein fold was similar to the structure of T252E-CYP199A4 (PDB: 7REH)[40] with an RMSD of 0.157 Å, Figure S1). There was electron density consistent with the mutated T252E residue and the retention of the 6th aqua ligand of the heme as observed with other T252E-CYP199A4 crystal structures (Figure 1).[38, 40] There was also electron density present within the active site consistent with the product bound as previously observed with other ligand-bound structures of CYP199A4.[41] This electron density was modelled as 4-hydroxybenzoic acid (occupancy 86%). The 4-hydroxybenzoic acid complex structure was superimposed to T252E-CYP199A4 complexed with 4-methoxybenzoic acid (PDB: 7REH, Figure S2). The active site structure between two complexes were similar with little or no differences observed between the positioning of key active site residues.

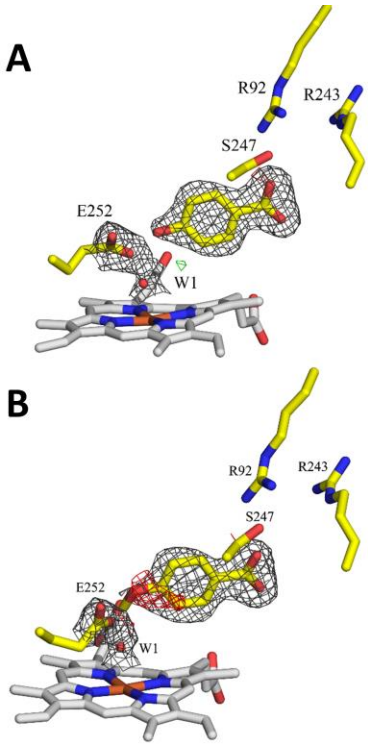

Figure 1. Crystal structure of T252E-CYP199A4 co-crystallised with 4-hydroxybenzoic acid (yellow sticks, PDB: 8GLY). In (a), the electron density of the bound substrate was modelled as 4-hydroxybenzoic and in (b) it was modelled as 4-methoxybenzoic acid. Composite-omit maps ($2mF_o$-F_c) are shown as a grey mesh contoured to 1.0 σ (1.5 Å carve) around the substrate, residue E252 and heme-bound water in (a) and (b). F_o-F_c maps contoured to 2.5 σ are also shown as a green or red mesh. In (b), there is a region of negative density (red mesh) around the methoxy functional group of would be located.

When the ligand was modelled as 4-hydroxybenzoic acid (Figure 1), the F_o-F_c maps showed no positive or negative density around the ligand indicating a good match. This was in contrast to when 4-methoxybenzoic acid was modelled (Figure 1), which showed a distinct region of negative density where the methoxy functional group would be modelled. This negative density clearly demonstrates that the additional atoms of 4-methoxybenzoic acid are a poor fit for the electron density of the 4-hydroxybenzoic acid product. A similar analysis was carried with T252E-CYP199A4 co-crystallised with 4-methoxybenzoic acid but modelled with 4-hydroxybenzoic acid instead (Figure S3). This demonstration of the difference in the F_o-F_c maps between the substrate ligand and the electron density of the product would assist in determining if the H_2O_2-soaked crystals of T252E-CYP199A4 underwent *O*-demethylation.

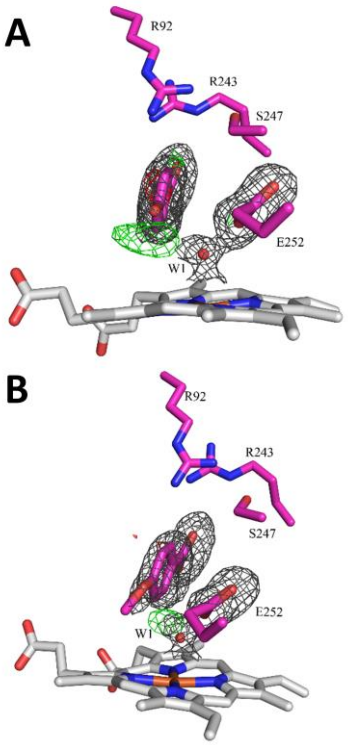

Figure 2. Crystal structure of T252E-CYP199A4 co-crystallised with 4-methoxybenzoic acid and soaked with 1 mM H_2O_2 for 0 min (magenta sticks, PDB: 8GM1). This structure was solved to a resolution of 1.85 Å. In (a), the electron density of the bound substrate was modelled as 4-hydroxybenzoic and in (b) it was modelled as 4-methoxybenzoic acid. Composite-omit maps (*2mF$_o$-F$_c$)* are shown as a grey mesh contoured to 1.0 σ (1.5 Å carve) around the substrate, residue E252 and heme-bound water in (a) and (b). F_o-F_c maps contoured to 2.5 σ are also shown as a green or red mesh.

The first structure solved for the *in crystallo* reactions was a crystal soaked with 1 mM H_2O_2 and flash-frozen immediately after addition of the peroxide (0 min). This structure was solved and refined to a resolution of 1.85 Å (PDB: 8GM1; Table S1 and Figure 2). When comparing the F_o-F_c maps between the two models, the 4-hydroxybenzoic acid model showed a large region of positive density (green mesh) surrounding the *para*-hydroxy moiety indicating the model used is missing atoms in this region (Figure 2). In the 4-methoxybenzoic acid model (Figure 2), no positive or negative density was observed near the *para* position of the bound ligand. This demonstrates that little or no demethylation of 4-methoxybenzoic acid had occurred within the crystal. It is noted that there is still a region of positive density above the heme and the aqua ligand in Figure 2. An attempt to model a H_2O_2 molecule above the heme resulted in negative density in the F_o-F_c map (Figure S7).

The other structures were from crystals soaked in H_2O_2, which were left for longer before being flash cooled. In the crystal structure of T252E-CYP199A4 with 4-methoxybenzoic acid, which was soaked with 4 mM of H_2O_2 for 5 min the F_o-F_c maps showed only a small region of positive density near the *para*-moiety when 4-hydroxybenzoic acid is the modelled ligand (resolution of 2.02 Å; PDB: 8GLZ; Figure 3). In the 4-methoxybenzoic acid model there was negative density around the *para*-methoxy moiety that indicates poor agreement between this model and the electron density (Figure 3).

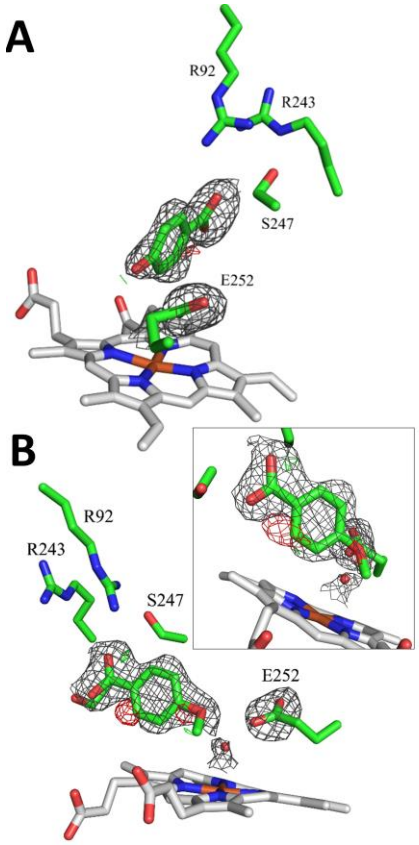

Figure 3. Crystal structure of T252E-CYP199A4 co-crystallised with 4-methoxybenzoic acid and soaked with 4 mM H_2O_2 for 5 min (green sticks, PDB: 8GLZ). This structure was solved to a resolution of 2.02 Å. In (a), the electron density of the bound substrate was modelled as 4-hydroxybenzoic acid and in (b) it was modelled as 4-methoxybenzoic acid. Composite-omit maps (*2mF$_o$-F$_c$*) are shown as a grey mesh contoured to 1.0 σ (1.5 Å carve) around the substrate, residue E252 and heme-bound water in (a) and (b). The F_o-F_c maps contoured to 2.5 σ are also shown as a green or red mesh.

For this structure, the F_o-F_c and composite-omit maps were similar to that of T252E-CYP199A4 bound to 4-hydroxybenzoic acid (Figure 1). Taken together this is strong evidence of 4-hydroxybenzoic acid bound within the active site. The positive density surrounding the 4-hydroxybenzoic acid model (Figure 3) is also significantly smaller in comparison to the crystal where little or no demethylation of the substrate occurred (Figure 2). This suggests that an *in crystallo* demethylation reaction has occurred after soaking with 4 mM H_2O_2.

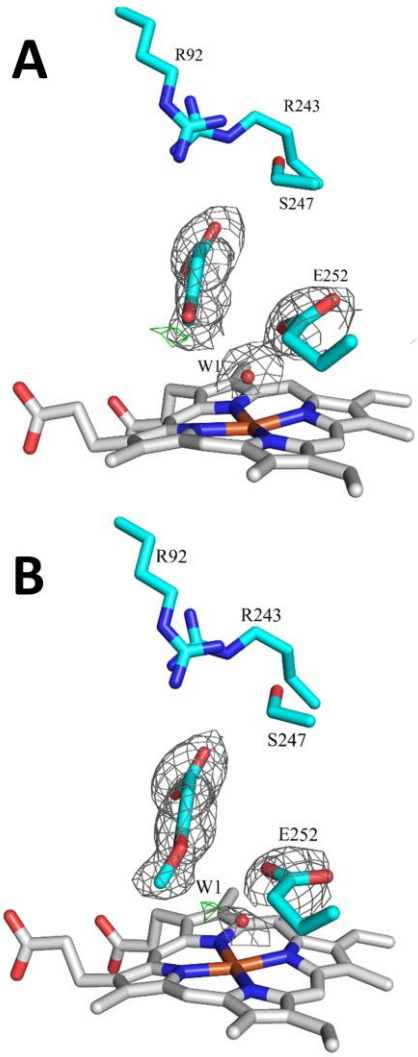

Figure 4. Crystal structure of T252E-CYP199A4 co-crystallised with 4-methoxybenzoic acid and soaked with 2 mM H_2O_2 for 10 min (cyan sticks, PDB: 8GM2). This structure was solved to a resolution of 2.33 Å. In (a), the electron density of the bound substrate was modelled as 4-hydroxybenzoic and in (b) it was modelled as 4-methoxybenzoic acid. Composite-omit maps ($2mF_o$-F_c) are shown as a grey mesh contoured to 1.0 σ (1.5 Å carve) around the substrate, residue E252 and heme-bound water in (a) and (b). F_o-F_c maps contoured to 2.5 σ are also shown as a green or red mesh.

The crystal structure of T252E-CYP199A4 bound to 4-methoxybenzoic acid that was soaked in 2 mM H_2O_2 for 10 min was determined at 2.33 Å resolution (PDB: 8GM2; Table S1 Figure 4). The model of both 4-hydroxybenzoic acid and 4-methoxybenzoic acid showed no significant regions of negative density. However, a small region of positive density was observed with the 4-hydroxybenzoic acid model (Figure 4). This shows that a lower proportion of the 4-methoxybenzoic acid ligand has undergone *O*-demethylation within this crystal (Figure 4) compared to that soaked with more H_2O_2 for a shorter period of time (Figure 3).

Modelling the electron density of the ligands bound to the different H_2O_2-soaked crystals with either 4-methoxybenzoic acid and 4-hydroxybenzoic acid suggests that different proportions of the initial substrate and demethylated metabolite were present in the T252E-CYP199A4 crystals. To further investigate the extent of the progress of the *in crystallo* enzymatic reaction, both 4-methoxybenzoic acid and 4-hydroxybenzoic acid were modelled in same location using different alternative location (altloc) identifiers and the occupancies of both ligands refined (Table 1).

Condition	Ligand Occupancy (%)	
	4-hydroxyBA	4-methoxyBA
4 mM H_2O_2/5 min (PDB:8GLZ)	70	30
2 mM H_2O_2/10 min (PDB: 8GM2)	35	62
1 mM H_2O_2/0 min (PDB: 8GM1)	47	50
4-hydroxyBA (PDB: 8GLY)	86	-
4-methoxyBA (PDB: 7REH)	-	100

Table 1. Occupancies of 4-methoxybenzoic acid and 4-hydroxybenzoic acid co-refined at the same location in H_2O_2 soaked crystals of T252E-CYP199A4.

The refined occupancies of the bound ligand to the soaked crystals were largely consistent with what was observed with the F_o-F_c maps (Figures 2-4). The 4 mM H_2O_2-soaked crystal showed the highest proportion of 4-hydroxybenzoic acid (70%, Table 1) which agrees with demethylation being observed with its respective F_o-F_c maps (Figure 3). Crystals soaked with 1 mM and 2 mM H_2O_2 showed less or no *in crystallo* demethylation occurring based on the F_o-F_c maps (Figure 2 and Figure 4). The occupancy of 4-methoxybenzoic acid for these two crystals was indeed higher compared to the demethylated product (Table 1). The proportion of 4-methoxybenzoic acid was highest in the crystal soaked in 2 mM H_2O_2 (62%) suggesting that *in crystallo* demethylation occurred to a lesser extent compared to the other conditions in these crystals.

The exposure of peroxide to P450 enzymes such as T252E-CYP199A4 and other P450 peroxygenases has been shown to damage the heme centre.[38,40,42] To assess if this peroxide-driven damage causes any changes with the H_2O_2-soaked crystals the crystals that were soaked with 4 mM H_2O_2 and 2 mM H_2O_2 for 5 min and 10 min respectively were modelled with their respective ligand with the highest refined occupancy in Table 1. Their active site structure of each crystal was compared a structure of T252E-CYP199A4 bound to 4-methoxybenzoic acid (PDB: 7REH) and T252E-

CYP199A4 with 4-hydroxybenzoic acid (PDB: 8GLY; Figure 5). The distances and angles of key active site features for these crystal structures were measured and compared (Table S2). The general features of the active site across all the structures were similar. The chloride capping anion is present alongside water molecules that interact with the heme and benzoic acid moiety of the ligand and there was no evidence of heme damage that would infer peroxide induced heme damage (Figure 5 and Figure S8).[40]

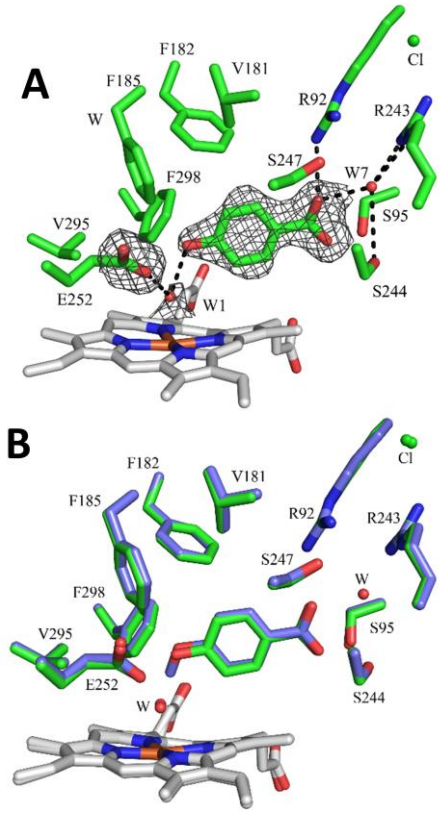

Figure 5. (a) The structure of T252E-CYP199A4 crystallised with 4-methoxybenzoic acid solved to 2.02 Å that underwent *in crystallo* demethylation after soaking with 4 mM H_2O_2 for 5 min (green sticks, PDB: 8GLZ). The ligand bound was modelled as 4-hydroxybenzoic acid. A composite-omit map ($2mF_o$-F_c) is shown around the bound ligand, residue E252 and heme-bound water (W1) as a grey mesh (1.0 σ, 1.5 Å carve) (b) Structure of T252E-CYP199A4 soaked with 4 mM H_2O_2 (green sticks) superimposed with the same enzyme complexed with 4-methoxybenzoic acid (navy sticks, PDB: 7REH).

When the structure of crystallised T252E-CYP199A4 soaked with 4 mM H_2O_2 for 5 min was modelled and refined with 4-hydroxybenzoic acid as the bound ligand (Figure 5, PDB: 8GLZ) the occupancy of the heme-bound water ligand was 88%. The active site structure of this H_2O_2-soaked crystal T252E-CYP199A4 also showed no significant differences with the previously reported structure of this enzyme (Figure 5, PDB: 7REH).

The crystal structure of T252E-CYP199A4 soaked with 2 mM H_2O_2 for 10 min (2.33 Å, PDB: 8GM2) was also compared to the structure of the same mutant complexed with 4-methoxybenzoic acid (PDB: 7REH; Figure S8) and 4-hydroxybenzoic acid (PDB: 8GLY Figure S8). The ligand of the H_2O_2-soaked structure was modelled as 4-methoxybenzoic acid and the heme-bound water had 100% occupancy (Figure 6). The active site conformation between the compared structures were largely similar. An altered conformation for mutated E252 residue was observed in this H_2O_2 soaked crystal (Figure 6 and Figure S8). The carboxylate of the E252 residue was oriented upwards by ~18° after soaking with H_2O_2 and becomes more in parallel with the plane of the heme (Figure S8).

In summary, three different crystals of T252E-CYP199A4 in complex with 4-methoxybenzoic acid were soaked in varying concentrations of H_2O_2 (Figure 6). The crystal of the T252E mutant soaked for 4 mM H_2O_2 for 5 mins showed a loss of electron density of the bound ligand that was consistent with *in crystallo* demethylation.

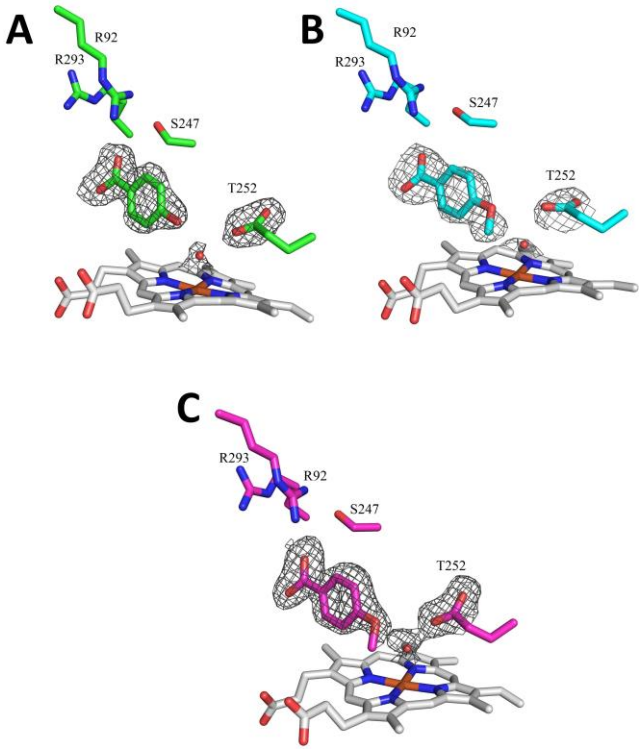

Figure 6: Crystal structures of T252E-CYP199A4 soaked with H_2O_2. In (a), crystal was soaked with 4 mM H_2O_2 for 5 mins and 4-hydroxybenzoic acid was the highest occupancy ligand observed. In (b) and (c), crystals were soaked with 2 mM and 1 mM H_2O_2 respectively while 4-methoxybenzoic acid was the highest occupancy ligand observed for both (b) and (c). Composite omit maps were shown as a grey mesh (1.0 σ, 1.5 Å carve).

Discussion

The structure of T252E-CYP199A4 in complex with 4-hydroxybenzoic acid has been solved for the first time. This ligand is a product of *O*-demethylation by CYP199A4 using 4-methoxybenzoic acid as a substrate. 4-Methoxybenzoic acid binds tightly to WT CYP199A4 (K_d = 0.3 μM)[30] and the T252E mutant (K_d = 1.1 μM)[40]. The binding affinity of 4-hydroxybenzoic acid is unknown but it would be expected to

bind less tightly. For example, the dissociation constants for $P450_{cam}$ with its physiological substrate, camphor (K_d = 0.25 μM)[43] showed it was bound nearly 40-fold tighter compared to the product, 5-*exo*-hydroxycamphor (K_d = ~ 10 μM).[44] From this, we can infer CYP199A4 and its mutant would behave similarly, whereby 4-hydroxybenzoic acid will bind less tightly to CYP199A4 compared to 4-methoxybenzoic acid. The refined occupancy of 4-hydroxybenzoic acid bound to T252E-CYP199A4 was found to be 86%. The ligand binding mode and active site geometry of T252E-CYP199A4 was not altered significantly with 4-hydroxybenzoic acid compared to 4-methoxybenzoic acid. A structure of $P450_{cam}$ bound to the hydroxylation product, 5-*exo*-hydroxycamphor found the product and substrate are held in a similar position.[5]

The structure of $P450_{cam}$ with 5-*exo*-hydroxycamphor also revealed an interaction between the product OH group and the heme-iron centre (Fe-O, ≈ 2.7 Å). The alcohol group of 4-hydroxybenzoic acid was much further away from the iron (Fe-O, 4.8 Å) and interacts with a heme-bound distal water ligand (83% occupancy). This was to be expected as other benzoic acid substrates were also unable to displace this heme-bound water in this mutant.[40] This is due to the distal water molecule interacting with the carboxylate of E252 (2.6 Å) and allows it to remain bound to the heme-iron.

In crystallo O-demethylation reactions were demonstrated with crystallised T252E-CYP199A4 bound to 4-methoxybenzoic acid and soaked with H_2O_2. The soaking condition that drove demethylation to the greatest degree being 4 mM H_2O_2 for 5 min and this was the highest concentration of H_2O_2 tested. Analysis revealed 4-hydroxybenzoic acid with an occupancy of 70%. The alternate soaking conditions of 2 mM H_2O_2 for 10 min drove *in crystallo* demethylation the least (35% occupancy of 4-hydroxybenzoic acid) compared to soaking in 1 mM H_2O_2 for 0 min (47% occupancy of 4-hydroxybenzoic acid). This discrepancy with the higher concentration of H_2O_2 forming less 4-hydroxybenzoic acid could be due to poorer diffusion of H_2O_2 into the crystal lattice. The rate of diffusion of molecules into the crystal lattice does not only depend on a high concentration of the soaked molecule during the soaking step but also the crystals need to be small with large diffusion coefficients.[45] The size of the crystal chosen for this study were chosen at random. Crystals with edge lengths in single digit μm or smaller are recommended for diffusion triggered *in crystallo* reactions.[45]

Further investigations could involve large-scale batch crystallisation to form microcrystals of T252E-CYP199A4. Facile crystallisation of microcrystals in batch have been achieved with different enzymes by incorporating ammonium sulfate precipitation to the vapor diffusion crystallisation conditions of these enzymes.[46] Microcrystals are susceptible to damage to X-ray radiation,[45] but large batches of microcrystals can be used for serial crystallography. This involves thousands of microcrystals being exposed to X-ray free electron lasers (XFEL) that damages the microcrystals but diffraction occurs at a femtosecond scale.[47] As diffraction is essentially instantaneous, large batches of crystals could be used in serial crystallography to obtain diffraction data for structure determination. Microcrystals of T252E-CYP199A4 used for H_2O_2 triggered *in crystallo* reactions could be investigated with serial crystallography to explore femtosecond resolved structures along the catalytic pathway of this enzyme.

Crystals with large diffusion coefficients would allow fast diffusion of the target molecule into the crystal lattice and is influenced by large, water-filled channels within the crystallised protein.[45] The size of the solvent pores within crystals of CYP199A4 has not been assessed. A possible approach to improve the diffusion of H_2O_2 into the crystals of this P450 enzyme would be analysing the solvent channels of the enzyme using CAVER 3.0.[48,49] For example, this method was used to identify and estimate the importance of the solvent channels in haloalkane dehalogenase DhaA for catalytic activity.[48]

In crystallo P450 reactions driven by the peroxide shunt has only been demonstrated with CYP121 with a synthetic probe designed to mimic its native substrate, cyclo(l-Tyr-l-Tyr) (cYY).[27] Soaking of CYP121 co-crystallised with the synthetic probe in H_2O_2 formed a hydroxylated intermediate that was potentially captured by X-ray crystallography (Figure S10). This hydroxylated intermediate was reported to share 50% occupancy with the substrate precursor thought this appeared less clear from the electron density (Figure S10). In our current study, the highest occupancy observed for an *in crystallo* demethylation product with T252E-CYP199A4 was 70%. Future work could include testing other substrates with crystallised T252E-CYP199A4 that could undergo different *in crystallo* P450 reactions such as hydroxylation and sulfoxidation. It is envisioned that trapping H_2O_2 within the crystallised enzyme could be achieved to assess how the peroxide molecule interacts with the active site residues. Trapping of a peroxide molecule with other iron containing enzymes has been shown to be possible.[50]

In summary, a crystal structure of T252E-CYP199A4 complexed with 4-hydroxybenzoic acid was solved for the first time. Active site geometry and ligand binding modes of enzyme complex did not differ significantly from when the enzyme was bound to 4-methoxybenzoic acid. *In crystallo O*-demethylation of 4-methoxybenzoic acid was demonstrated for the first time within crystals of T252E-CYP199A4.

Experimental Section

General reagents and organics were purchased from Sigma-Aldrich. Isopropyl-β-D-thiogalactopyranoside (IPTG) and buffer components were obtained from Astral Scientific (Australia). UV/Vis spectra and spectroscopic activity assays were performed on an Agilent Cary 60 spectrophotometer at 30 ± 5 °C.

Production and Purification of T252E-CYP199A4. Mutant T252E of CYP199A4 was expressed as previously described but with the addition of 4-methoxybenzoic acid to a concentration of 1 mM to the expression media before induction. The expressed protein was then purified using previously established methods.[40] Proteins were stored in 50% v/v glycerol at -20 °C.

Protein Crystallography and *In Crystallo* Enzymatic Reactions. Crystallisation experiments were performed with T252E-CYP199A4. Immediately prior to preparation of crystal trays, the protein was purified via elution through a HiPrep Sephacryl S-200 HR size-exclusion column (60 cm x 16 mm; GE Healthcare) with Buffer T at a flow rate of 1 mL min^{-1}. The purity of the protein was assessed based on the Reinheitszahl value, RZ = A_{420}/A_{280}, whereby fractions with RZ = 2 were collected and combined.

Substrate (4-methoxy- or 4-hydroxybenzoic acid) in DMSO was then added to the combined fractions to a final concentration of 1 mM from a 100 mM stock to the concentrated protein. The combined fractions with substrate were incubated at 4 °C and then concentrated via ultrafiltration using a Microsep Advance centrifugal device (10 kDa MWCO, Pall Corporation) to a concentration of approximately 30 – 35 mg mL^{-1}. Crystallisation trays were prepared using the following optimised buffer conditions previously reported: 0.2 M magnesium acetate, 100 mM Bis-Tris buffer (adjusted with acetic acid to pH 5.0 - 5.75) and 20 - 32% w/v polyethylene glycol (PEG) 3350.[41] Protein crystallisation was achieved using the hanging-drop vapor diffusion method in 24-well trays. An equal volume of crystallisation buffer was mixed with hanging drops of 1.2 - 2 µL of protein and was equilibrated with a reservoir of the same buffer (500 µL) at 16 °C. Red plate-like crystals were obtained after half a day to one week.

In crystallo reactions were carried out with T252E-CYP199A4 co-crystallised with 4-methoxybenzoic acid. Single crystals were picked from individual wells and soaked in their respective crystallisation buffer containing H_2O_2. The crystals were soaked at different concentrations of H_2O_2 (0.5 to 10 mM) with variable soaking times (0, 5 and 10 min). After soaking, single crystals were mounted onto Micromounts or Microloops (MiTeGen LLC, New York, USA). Mounted crystals were immersed in Parabar 10312 Oil (Paratone-N, Hampton Research, California, USA) before flash-cooled in liquid N_2.

X-ray diffraction data were obtained (360 images per crystal) at the Australian Synchrotron using the MX1 beamline[51] with an exposure time of 1 s, oscillation angle of 1 °, wavelength of 0.9537 Å and temperature of 100 K. Diffraction images were indexed and integrated using iMosfilm. [52] Aimless[53] from the CCP_4 suite of programs[54] was used to carry out scaling, merging and R_{free} labelling (5% of reflections, randomly selected). The phase problem was solved using Molecular Replacement in Phaser[55] using a high-resolution structure of WT CYP199A4 (1.54 Å, PDB: 5UVB) as the search model. The ligands and solvent molecules were removed from the search model prior to phasing to eliminate model bias. Weighted $2mF_o$-F_c maps and F_o-F_c difference maps were obtained and used to rebuild the model in WinCoot and determine the substrate binding mode.[56] Structural refinements were carried out over multiple cycles using Phenix Refine, available in the Phenix suite of programs.[57]

Composite-omit or feature enhanced maps that reduce model bias were generated in Phenix to allow inspection of the ligand binding site and reveal the location of all substrate atoms.[58, 59] Detailed data collection and structural refinement statistics are provided in the supporting information. To model the location of the Cpd I oxygen atom (Table S2), the CreateAtomAlongBond script was employed. Computational studies of Cpd I have calculated that the Fe-O bond length is very consistent at 1.62 Å. This was determined both in the absence and in the presence of substrate for CYPs 2C9, 2D6, 3A4 and $P450_{cam}$.[60] The oxygen atom was thus positioned 1.62 Å from the heme iron of the CYP199A4 structures.

Author Information

Corresponding Author

*Stephen G. Bell
Department of Chemistry, University Adelaide, Adelaide, SA, 5005, Australia
E-mail: stephen.bell@adelaide.edu.au

Acknowledgements

The authors acknowledge the Australian Government for Research Training Program Scholarships (PhD to JHZL). JHZL thanks the University of Adelaide for a Constance Fraser PhD Scholarship and the CSIRO Synthetic Biology Future Science Platform for a PhD top-up Scholarship. We would like to thank the scientists at the MX1 beamline at the Australian Synchrotron for help with data collection. We acknowledge ANSTO for financial support and in providing the facility used in this work. The authors thank Dr Tom Coleman for a photo of crystallised CYP199A4.

Notes

The authors declare no competing financial interest.

References

(1) Guengerich, F. P. New Trends in Cytochrome P450 Research at the Half-Century Mark. *J. Biol. Chem.* **2013**, *288* (24), 17063-17064, https://doi.org/10.1074/jbc.R113.466821.
(2) Sirim, D.; Wagner, F.; Lisitsa, A.; Pleiss, J. The Cytochrome P450 Engineering Database: integration of biochemical properties. *BMC Biochem.* **2009**, *10* (1), https://doi.org/10.1186/1471-2091-10-27.
(3) Sirim, D.; Widmann, M.; Wagner, F.; Pleiss, J. Prediction and analysis of the modular structure of cytochrome P450 monooxygenases. *BMC Struct. Biol.* **2010**, *10* (1), https://doi.org/10.1186/1472-6807-10-34.
(4) Poulos, T. L.; Finzel, B. C.; Gunsalus, I. C.; Wagner, G. C.; Kraut, J. The 2.6-A crystal structure of Pseudomonas putida cytochrome P-450. *J. Biol. Chem.* **1985**, *260* (30), 16122-16130.
(5) Li, H.; Narasimhulu, S.; Havran, L. M.; Winkler, J. D.; Poulos, T. L. Crystal Structure of Cytochrome P450cam Complexed with Its Catalytic Product, 5-exo-Hydroxycamphor. *J. Am. Chem. Soc.* **1995**, *117* (23), 6297-6299, https://doi.org/10.1021/ja00128a019.
(6) Poulos, T. L.; Finzel, B. C.; Howard, A. J. Crystal structure of substrate-free Pseudomonas putida cytochrome P-450. *Biochemistry (Mosc.)* **1986**, *25* (18), 5314-5322, https://doi.org/10.1021/bi00366a049.
(7) Raag, R.; Poulos, T. L. Crystal structure of the carbon monoxide-substrate-cytochrome P450cam ternary complex. *Biochemistry (Mosc.)* **1989**, *28* (19), 7586-7592, https://doi.org/10.1021/bi00445a013.

(8) Poulos, T. L.; Johnson, E. F. Structures of Cytochrome P450 Enzymes. Ortiz de Montellano, P. R., Ed.; Springer US: 2005; pp 87-114.
(9) Poulos, T. L.; Johnson, E. F. Structures of Cytochrome P450 Enzymes. In *Cytochrome P450*, Springer International Publishing, 2015; pp 3-32.
(10) Poulos, T. L.; Follmer, A. H. Updating the Paradigm: Redox Partner Binding and Conformational Dynamics in Cytochromes P450. *Acc. Chem. Res.* **2022**, *55* (3), 373-380. DOI: 10.1021/acs.accounts.1c00632.
(11) Denisov, I. G.; Makris, T. M.; Sligar, S. G.; Schlichting, I. Structure and Chemistry of Cytochrome P450. *Chem. Rev.* **2005**, *105* (6), 2253-2278. DOI: 10.1021/cr0307143.
(12) Stoddard, B. L. Intermediate trapping and laue X-ray diffraction: Potential for enzyme mechanism, dynamics, and inhibitor screening. *Pharmacol. Ther.* **1996**, *70* (3), 215-256, https://doi.org/10.1016/0163-7258(96)00058-7.
(13) Schlichting, I.; Goody, R. S. [24] Triggering methods in crystallographic enzyme kinetics. In *Methods in Enzymology*, Elsevier, 1997; pp 467-490.
(14) Murarka, V. C.; Batabyal, D.; Amaya, J. A.; Sevrioukova, I. F.; Poulos, T. L. Unexpected Differences between Two Closely Related Bacterial P450 Camphor Monooxygenases. *Biochemistry* **2020**, *59* (29), 2743-2750. DOI: 10.1021/acs.biochem.0c00366.
(15) Batabyal, D.; Poulos, T. L. Crystal Structures and Functional Characterization of Wild-Type CYP101D1 and Its Active Site Mutants. *Biochemistry* **2013**, *52* (49), 8898-8906. DOI: 10.1021/bi401330c.
(16) Tripathi, S.; Li, H.; Poulos, T. L. Structural Basis for Effector Control and Redox Partner Recognition in Cytochrome P450. *Science (New York, N.Y.)* **2013**, *340* (6137), 1227-1230. DOI: 10.1126/science.1235797 (acccessed 2023/08/11).
(17) Schlichting, I.; Berendzen, J.; Chu, K.; Stock, A. M.; Maves, S. A.; Benson, D. E.; Sweet, R. M.; Ringe, D.; Petsko, G. A.; Sligar, S. G. The Catalytic Pathway of Cytochrome P450cam at Atomic Resolution. *Science (New York, N.Y.)* **2000**, *287* (5458), 1615-1622, https://doi.org/10.1126/science.287.5458.1615.
(18) Rittle, J.; Green, M. T. Cytochrome P450 Compound I: Capture, Characterization, and C-H Bond Activation Kinetics. *Science (New York, N.Y.)* **2010**, *330* (6006), 933-937, https://doi.org/10.1126/science.1193478.
(19) Hrycay, E. G.; Bandiera, S. M. Monooxygenase, Peroxidase and Peroxygenase Properties and Reaction Mechanisms of Cytochrome P450 Enzymes. In *Monooxygenase, Peroxidase and Peroxygenase Properties and Mechanisms of Cytochrome P450*, Springer International Publishing, 2015; pp 1-61.
(20) Harlington, A. C.; Shearwin, K. E.; Bell, S. G.; Whelan, F. Efficient ?-demethylation of lignin monoaromatics using the peroxygenase activity of cytochrome P450 enzymes. *Chemical communications (Cambridge, England)* **2022**, *58* (96), 13321-13324, https://doi.org/10.1039/d2cc04698a.
(21) Shoji, O.; Wiese, C.; Fujishiro, T.; Shirataki, C.; Wünsch, B.; Watanabe, Y. Aromatic C–H bond hydroxylation by P450 peroxygenases: a facile colorimetric assay for monooxygenation activities of enzymes based on Russig's blue formation. *J. Biol. Inorg. Chem.* **2010**, *15* (7), 1109-1115, https://doi.org/10.1007/s00775-010-0671-9.
(22) Fujishiro, T.; Shoji, O.; Nagano, S.; Sugimoto, H.; Shiro, Y.; Watanabe, Y. Crystal Structure of H2O2-dependent Cytochrome P450SPα with Its Bound Fatty Acid Substrate. *J. Biol. Chem.* **2011**, *286* (34), 29941-29950, https://doi.org/10.1074/jbc.m111.245225.
(23) Onoda, H.; Tanaka, S.; Watanabe, Y.; Shoji, O. Exploring hitherto uninvestigated reactions of the fatty acid peroxygenase CYP152A1: catalase reaction and Compound I formation. *Faraday Discuss.* **2022**, *234* (0), 304-314.
(24) Shoji, O.; Watanabe, Y. Peroxygenase reactions catalyzed by cytochromes P450. *J. Biol. Inorg. Chem.* **2014**, *19* (4-5), 529-539, https://doi.org/10.1007/s00775-014-1106-9.
(25) Shoji, O.; Fujishiro, T.; Nishio, K.; Kano, Y.; Kimoto, H.; Chien, S.-C.; Onoda, H.; Muramatsu, A.; Tanaka, S.; Hori, A.; et al. A substrate-binding-state mimic of H2O2-dependent cytochrome P450 produced by one-point mutagenesis and peroxygenation of non-native substrates. *Catal. Sci. Technol.* **2016**, *6*, 5806-5811, https://doi.org/10.1039/C6CY00630B.
(26) Onoda, H.; Shoji, O.; Suzuki, K.; Sugimoto, H.; Shiro, Y.; Watanabe, Y. α-Oxidative decarboxylation of fatty acids catalysed by cytochrome P450 peroxygenases yielding shorter-alkyl-chain fatty acids. *Catal. Sci. Technol.* **2018**, *8* (2), 434-442, https://doi.org/10.1039/c7cy02263h.
(27) Nguyen, R. C.; Yang, Y.; Wang, Y.; Davis, I.; Liu, A. Substrate-Assisted Hydroxylation and O-Demethylation in the Peroxidase-like Cytochrome P450 Enzyme CYP121. *ACS Catal.* **2019**, *10* (2), 1628-1639, https://doi.org/10.1021/acscatal.9b04596.
(28) Perkins, A.; Parsonage, D.; Nelson, K. J.; Ogba, O. M.; Cheong, P. H.-Y.; Poole, L. B.; Karplus, P. A. Peroxiredoxin Catalysis at Atomic Resolution. *Structure* **2016**, *24* (10), 1668-1678, https://doi.org/10.1016/j.str.2016.07.012.
(29) Bell, S. G.; Yang, W.; Tan, A. B. H.; Zhou, R.; Johnson, E. O. D.; Zhang, A.; Zhou, W.; Rao, Z.; Wong, L.-L. The crystal structures of 4-methoxybenzoate bound CYP199A2 and CYP199A4: structural changes on substrate binding and the identification of an anion binding site. *Dalton Trans.* **2012**, *41* (28), 8703-8714.
(30) Bell, S. G.; Zhou, R.; Yang, W.; Tan, A. B. H.; Gentleman, A. S.; Wong, L.-L.; Zhou, W. Investigation of the Substrate Range of CYP199A4: Modification of the Partition between Hydroxylation and Desaturation Activities by Substrate and Protein Engineering. *Chem. Eur. J.* **2012**, *18* (52), 16677-16688, https://doi.org/10.1002/chem.201202776.
(31) Coleman, T.; Chao, R. R.; Bruning, J. B.; De Voss, J. J.; Bell, S. G. CYP199A4 catalyses the efficient demethylation and demethenylation of para-substituted benzoic acid derivatives. *RSC Adv.* **2015**, *5*, 52007-52018, https://doi.org/10.1039/C5RA08730A.
(32) Coleman, T.; Wong, S. H.; Podgorski, M. N.; Bruning, J. B.; De Voss, J. J.; Bell, S. G. Cytochrome P450 CYP199A4 from Rhodopseudomonas palustris Catalyzes Heteroatom Dealkylations, Sulfoxidation, and Amide and Cyclic Hemiacetal Formation. *ACS Catal.* **2018**, *8* (7), 5915-5927, https://doi.org/10.1021/acscatal.8b00909.
(33) Coleman, T.; Kirk, A. M.; Lee, J. H. Z.; Doherty, D. Z.; Bruning, J. B.; Krenske, E. H.; Voss, J. J. D.; Bell, S. G. Different Geometric Requirements for Cytochrome P450-Catalyzed Aliphatic Versus Aromatic Hydroxylation Results in Chemoselective Oxidation. *ACS Catal.* **2022**, *12* (2), 1258-1267, https://doi.org/10.1021/acscatal.1c05483.
(34) Coleman, T.; Lee, J. Z. H.; Kirk, A. M.; Doherty, D. Z.; Podgorski, M. N.; Pinidiya, D. K.; Bruning, J. B.; Voss, J. J. D.; Krenske, E. H.; Bell, S. G. Enabling Aromatic Hydroxylation in a Cytochrome P450 Monooxygenase Enzyme through Protein Engineering. *Chem. Eur. J.* **2022**, *28* (67), https://doi.org/10.1002/chem.202201895.
(35) Coleman, T.; Doherty, D. Z.; Zhang, T.; Podgorski, M. N.; Qiao, R.; Lee, J. H. Z.; Bruning, J. B.; Voss, J. J. D.; Zhou, W.; Bell, S. G. Exploring the Factors which Result in Cytochrome P450 Catalyzed Desaturation Versus Hydroxylation. *Chem. Asian J.* **2022**, https://doi.org/10.1002/asia.202200986.

(36) Podgorski, M. N.; Coleman, T.; Churchman, L. R.; Bruning, J. B.; Voss, J. J. D.; Bell, S. G. Investigating the active oxidants involved in cytochrome P450 catalyzed sulfoxidation reactions. *Chem. Eur. J.* **2022**, Accepted-Accepted, https://doi.org/10.1002/chem.202202428.
(37) Podgorski, M. N.; Harbort, J. S.; Coleman, T.; Stok, J. E.; Yorke, J. A.; Wong, L.-L.; Bruning, J. B.; Bernhardt, P. V.; Voss, J. J. D.; Harmer, J. R.; et al. Biophysical Techniques for Distinguishing Ligand Binding Modes in Cytochrome P450 Monooxygenases. *Biochemistry* **2020**, *59* (9), 1038-1050, https://doi.org/10.1021/acs.biochem.0c00027.
(38) Lee, J. H. Z.; Podgorski, M. N.; Moir, M.; Gee, A. R.; Bell, S. G. Selective Oxidations Using a Cytochrome P450 Enzyme Variant Driven with Surrogate Oxygen Donors and Light. *Chem. Eur. J.* **2022**, *28* (49), https://doi.org/10.1002/chem.202201366.
(39) Coleman, T.; Kirk, A. M.; Chao, R. R.; Podgorski, M. N.; Harbort, J. S.; Churchman, L. R.; Bruning, J. B.; Bernhardt, P. V.; Harmer, J. R.; Krenske, E. H.; et al. Understanding the Mechanistic Requirements for Efficient and Stereoselective Alkene Epoxidation by a Cytochrome P450 Enzyme. *ACS Catal.* **2021**, *11* (4), 1995-2010, https://doi.org/10.1021/acscatal.0c04872.
(40) Podgorski, M. N.; Harbort, J. S.; Lee, J. H. Z.; Nguyen, G. T. H.; Bruning, J. B.; Donald, W. A.; Bernhardt, P. V.; Harmer, J. R.; Bell, S. G. An Altered Heme Environment in an Engineered Cytochrome P450 Enzyme Enables the Switch from Monooxygenase to Peroxygenase Activity. *ACS Catal.* **2022**, *12* (3), 1614-1625, https://doi.org/10.1021/acscatal.1c05877.
(41) Coleman, T.; Chao, R. R.; Voss, J. J. D.; Bell, S. G. The importance of the benzoic acid carboxylate moiety for substrate recognition by CYP199A4 from Rhodopseudomonas palustris HaA2. *Biochim. Biophys. Acta, Proteins Proteomics* **2016**, *1864* (6), 667-675, https://doi.org/10.1016/j.bbapap.2016.03.006.
(42) Dornevil, K.; Davis, I.; Fielding, A. J.; Terrell, J. R.; Ma, L.; Liu, A. Cross-linking of dicyclotyrosine by the cytochrome P450 enzyme CYP121 from Mycobacterium tuberculosis proceeds through a catalytic shunt pathway. *J. Biol. Chem.* **2017**, *292* (33), 13645-13657, https://doi.org/10.1074/jbc.m117.794099.
(43) Bell, S. G.; Orton, E.; Boyd, H.; Stevenson, J.-A.; Riddle, A.; Campbell, S.; Wong, L.-L. Engineering cytochrome P450cam into an alkane hydroxylase. *Dalton Trans.* **2003**, (11), 2133-2133, https://doi.org/10.1039/b300869j.
(44) Atkins, W. M.; Sligar, S. G. The roles of active site hydrogen bonding in cytochrome P-450cam as revealed by site-directed mutagenesis. *J. Biol. Chem.* **1988**, *263* (35), 18842-18849.
(45) Schmidt, M. Reaction Initiation in Enzyme Crystals by Diffusion of Substrate. *Crystals* **2020**, *10* (2), 116-116, https://doi.org/10.3390/cryst10020116.
(46) Stohrer, C.; Horrell, S.; Meier, S.; Sans, M.; von Stetten, D.; Hough, M.; Goldman, A.; Monteiro, D. C. F.; Pearson, A. R. Homogeneous batch micro-crystallization of proteins from ammonium sulfate. *Acta Crystallogr. D* **2021**, *77* (2), 194-204, https://doi.org/10.1107/s2059798320015454.
(47) Hough, M. A.; Owen, R. L. Serial synchrotron and XFEL crystallography for studies of metalloprotein catalysis. *Curr. Opin. Struct. Biol.* **2021**, *71*, 232-238, https://doi.org/10.1016/j.sbi.2021.07.007.
(48) Chovancova, E.; Pavelka, A.; Benes, P.; Strnad, O.; Brezovsky, J.; Kozlikova, B.; Gora, A.; Sustr, V.; Klvana, M.; Medek, P.; et al. CAVER 3.0: A Tool for the Analysis of Transport Pathways in Dynamic Protein Structures. *PLoS Comput. Biol.* **2012**, *8* (10), e1002708-e1002708, https://doi.org/10.1371/journal.pcbi.1002708.
(49) Zhao, P.; Kong, F.; Jiang, Y.; Qin, X.; Tian, X.; Cong, Z. Enabling Peroxygenase Activity in Cytochrome P450 Monooxygenases by Engineering Hydrogen Peroxide Tunnels. *J. Am. Chem. Soc.* **2023**, *145* (9), 5506-5511. DOI: 10.1021/jacs.3c00195.
(50) Bailey, L. J.; Fox, B. G. Crystallographic and Catalytic Studies of the Peroxide-Shunt Reaction in a Diiron Hydroxylase. *Biochemistry* **2009**, *48* (38), 8932-8939, https://doi.org/10.1021/bi901150a.
(51) Cowieson, N. P.; Aragao, D.; Clift, M.; Ericsson, D. J.; Gee, C.; Harrop, S. J.; Mudie, N.; Panjikar, S.; Price, J. R.; Riboldi-Tunnicliffe, A.; et al. MX1: a bending-magnet crystallography beamline serving both chemical and macromolecular crystallography communities at the Australian Synchrotron. *J. Synchrotron Radiat.* **2015**, *22* (1), 187-190, https://doi.org/10.1107/s1600577514021717.
(52) Battye, T. G. G.; Kontogiannis, L.; Johnson, O.; Powell, H. R.; Leslie, A. G. W. iMOSFLM: a new graphical interface for diffraction-image processing with MOSFLM. *Acta Crystallogr. D* **2011**, *67* (4), 271-281, https://doi.org/10.1107/s0907444910048675.
(53) Evans, P. R.; Murshudov, G. N. How good are my data and what is the resolution? *Acta Crystallogr. D* **2013**, *69* (7), 1204-1214, https://doi.org/10.1107/s0907444913000061.
(54) Winn, M. D.; Ballard, C. C.; Cowtan, K. D.; Dodson, E. J.; Emsley, P.; Evans, P. R.; Keegan, R. M.; Krissinel, E. B.; Leslie, A. G. W.; McCoy, A.; et al. Overview of the CCP_4 suite and current developments. *Acta Crystallogr. D* **2011**, *67* (4), 235-242, https://doi.org/10.1107/s0907444910045749.
(55) McCoy, A. J.; Grosse-Kunstleve, R. W.; Adams, P. D.; Winn, M. D.; Storoni, L. C.; Read, R. J. Phaser crystallographic software. *J. Appl. Crystallogr.* **2007**, *40* (4), 658-674, https://doi.org/10.1107/s0021889807021206.
(56) Emsley, P.; Lohkamp, B.; Scott, W. G.; Cowtan, K. Features and development of Coot. *Acta Crystallogr. D* **2010**, *66* (4), 486-501, https://doi.org/10.1107/s0907444910007493.
(57) Adams, P. D.; Afonine, P. V.; Bunkóczi, G.; Chen, V. B.; Davis, I. W.; Echols, N.; Headd, J. J.; Hung, L.-W.; Kapral, G. J.; Grosse-Kunstleve, R. W.; et al. PHENIX: a comprehensive Python-based system for macromolecular structure solution. *Acta Crystallogr. D* **2010**, *66* (2), 213-221, https://doi.org/10.1107/s0907444909052925.
(58) Terwilliger, T. C.; Grosse-Kunstleve, R. W.; Afonine, P. V.; Moriarty, N. W.; Adams, P. D.; Read, R. J.; Zwart, P. H.; Hung, L.-W. Iterative-build OMIT maps: map improvement by iterative model building and refinement without model bias. *Acta Crystallogr. D* **2008**, *64* (5), 515-524, https://doi.org/10.1107/s0907444908004319.
(59) Afonine, P. V.; Moriarty, N. W.; Mustyakimov, M.; Sobolev, O. V.; Terwilliger, T. C.; Turk, D.; Urzhumtsev, A.; Adams, P. D. FEM: feature-enhanced map. *Acta Crystallogr. D* **2015**, *71* (3), 646-666, https://doi.org/10.1107/s1399004714028132.
(60) Lonsdale, R.; Oláh, J.; Mulholland, A. J.; Harvey, J. N. Does Compound I Vary Significantly between Isoforms of Cytochrome P450? *J. Am. Chem. Soc.* **2011**, *133* (39), 15464-15474, https://doi.org/10.1021/ja203157u.

For Table of Contents Only